RAPID COMMUNICATIONS

PHYSICAL REVIEW B VOLUME 52, NUMBER 12 15 SEPTEMBER 1995-II

Cyclotron-resonance anomalies in an antidot array measured by microwave photoconductivity

E. Vasiliadou
Max-Planck-Institut für Festkörperforschung, D-70569 Stuttgart, Germany

R. Fleischmann
Institut für Theoretische Physik, Universität Frankfurt, D-60054 Frankfurt/Main, Germany

D. Weiss
Max-Planck-Institut für Festkörperforschung, D-70569 Stuttgart, Germany

D. Heitmann
Institut für Angewandte Physik, Universität Hamburg, D-20355 Hamburg, Germany

K. v. Klitzing
Max-Planck-Institut für Festkörperforschung, D-70569 Stuttgart, Germany

T. Geisel
Institut für Theoretische Physik, Universität Frankfurt, D-60054 Frankfurt/Main, Germany

R. Bergmann and H. Schweizer
4. Physikalisches Institut der Universität Stuttgart, D-70550 Stuttgart, Germany

C. T. Foxon
Department of Physics, University of Nottingham, Nottingham NG7 2RD, United Kingdom
(Received 2 May 1995)

A lateral antidot array with a lattice period of 400 nm fabricated with electron-beam lithography on GaAs/$Al_xGa_{1-x}As$ heterostructures was investigated by microwave photoconductivity. Commensurability effects and distinct deviations from the classical cyclotron resonance have been observed in agreement with model calculations based on nonlinear dynamics of the electrons.

A two-dimensional electron system (2DES) embedded in an array of strong repulsive potential pillars is called an antidot array. Such systems are typically fabricated from a high-mobility 2DES by etching a grid of holes through the two-dimensional electron gas.[1,2] The resulting potential posts are higher than the Fermi energy in the 2DES and hence define classically forbidden regions for the electrons. The electron motion between the periodically arranged artificial scatterers results in distinct resistance anomalies at low temperatures.[2] The dominant features in transport experiments are, as a function of the applied magnetic field B, pronounced resistance peaks which arise when the classical cyclotron radius r_c at the Fermi energy fits around a particular number of antidots (1,2,4,9, . . . in a square array). The motion of the electrons is in general chaotic and a detailed description of the resistance requires an elaborate analysis of the electron motion. The result of such calculations[3] explains features in the experiment that are not covered by the simple circular orbit analysis mentioned above.[2] The fact that the antidot posts are not steep but emerge softly from the bottom of the conduction band is the origin of distorted cyclotron orbits that show up in transport experiments. These noncircular cyclotron orbits corresponding to nonlinear resonances in phase space are expected to cause deviations from the usual frequency $f_c = eB/2\pi m^*$ (m^* is the effective mass in GaAs) of the cyclotron motion.[3,4] A study of the cyclotron resonance in antidot systems should therefore directly reflect the signatures of the nonlinear dynamics of the electrons.

The typical experimental method to detect such anomalies is far-infrared (FIR) transmission spectroscopy. Experiments for wave numbers larger than 15 cm^{-1} have been carried out previously.[1] They show two dominant modes for the dynamic response in a perpendicular magnetic field B. To detect commensurability effects at low magnetic fields optically it is necessary to work in the microwave regime. Microwave transmission and reflection experiments in general require complex techniques to eliminate multiple reflections of the waves between the surfaces inside of the sample and the sample holder;[5] they also require large patterned areas. Therefore we use here a microwave photoconductivity experiment on a small Hall bar, which is much less affected by these difficulties.[6–8]

We prepared a standard Hall bar geometry (inset in Fig. 2) from a high-mobility GaAs/$Al_xGa_{1-x}As$ heterostructure. A rectangular field on the left Hall bar is patterned with an antidot grid of period $a = 400$ nm. The antidots were fabricated by electron-beam lithography and transferred to the 2DES by reactive ion etching. The right-hand part of the Hall bar is unpatterned and serves as a reference. The mobility μ of the unpatterned 2DES is 3.5×10^6 $cm^2/V\,s$ and that of the antidot region is 1.9×10^5 $cm^2/V\,s$ measured at $T = 1.3$ K with an electron density $N_s = 2.0\times10^{11}$ cm^{-2} for both regions.

Our photoconductivity measurements were performed with a double lock-in technique.[7,8] We used different back-

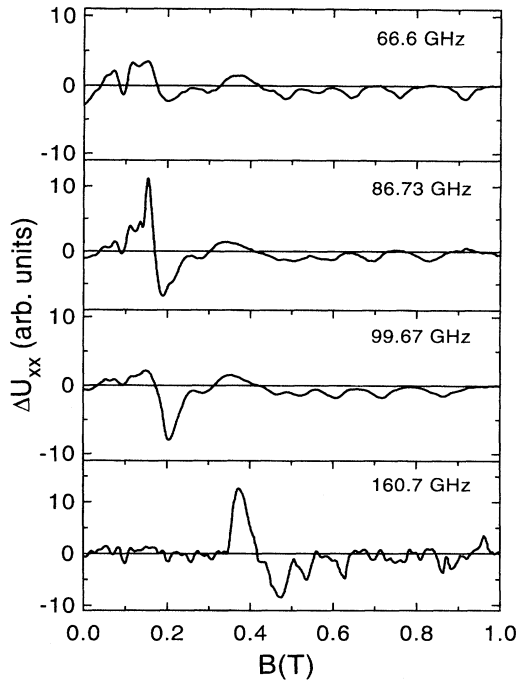

FIG. 1. Set of measured photoconductivity signals ΔU_{xx} vs B taken from the antidot region of the Hall bar at several fixed frequencies. Despite the complicated nonresonant background, discussed in the text, a clear resonant signal is observable, which shifts to higher B with increasing frequency.

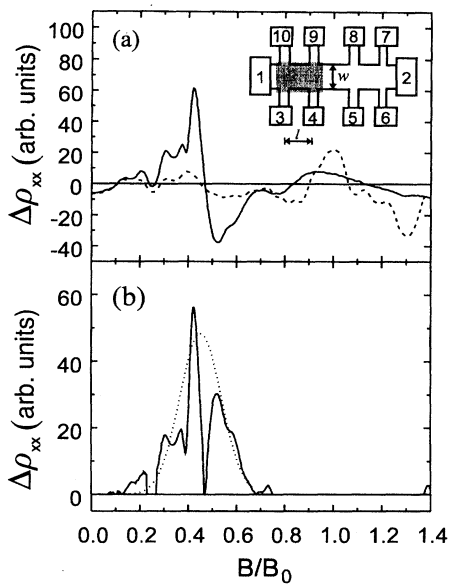

FIG. 2. Inset: Hall bar with patterned (shaded) and unpatterned segments. The period of the antidot lattice is $a=400$ nm and the geometrical antidot diameter is $d_{AD}=80$ nm. Here, $w=100$ μm, $l=200$ μm, and $B_0=0.37$ T. (a) Dashed line: $\alpha\Delta\rho_{xx}^T=\alpha[\rho_{xx}(1.2\ \mathrm{K})-\rho_{xx}(4.2\ \mathrm{K})]$ matched to the photosignal $\Delta\rho_{xx}$ (solid line) for $f=86.7$ GHz. (b) Solid line: absolute value of the resonant part of the photosignal; dotted line: Gaussian fit used to determine the resonance position.

ward wave oscillators and carcinotrons which generate microwave frequencies in the range from 60 to 166 GHz and from 230 to 390 GHz. The experiments were carried out at 1.3 K. The amplitude of the sinusoidal current driven through the contacts (1,2) of the Hall bar was 20 μA. With our sample design we can measure the induced photovoltage ΔU_{xx} either in the antidot region using contact pairs (3,4) and (10,9) or in the 2DES using (5,6) and (8,7).

A set of photosignals measured at several fixed frequencies is plotted in Fig. 1 as ΔU_{xx} vs B. We observe resonant signals which shift to higher magnetic fields with increasing microwave frequency. The resonances are superposed to a *nonresonant* background which originates from heating of the whole sample, including metallic contact pads and leads. The shape of this background signal is given by the difference $\Delta\rho_{xx}^T$ of ρ_{xx} at different temperatures. We used $\rho_{xx}(1.2\ \mathrm{K})-\rho_{xx}(4.2\ \mathrm{K})=\Delta\rho_{xx}^T$ to subtract the background from the measured data, assuming that the shape of the nonresonant signal is similar for all frequencies and intensities used. To extract the resonant signal we first match $\Delta\rho_{xx}^T$ to the photosignal $\Delta\rho_{xx}^{\mathrm{MW}}$ [solid line in Fig. 2(a)] by multiplying with a factor α such that both traces are equal at very small $B\leq 0.15$ T.[9] The matched trace $\alpha\Delta\rho_{xx}^T$, displayed in Fig. 2(a) as a dashed line, alternates around zero. This alternating behavior is due to the temperature dependence of the ρ_{xx} traces measured in antidot arrays: The maxima get reduced while the minima increase with increasing temperature. At magnetic fields where $\Delta\rho_{xx}^T\approx 0$, the sample is insensitive to microwave radiation. To account for this alternating signal we use the absolute value $|\Delta\rho_{xx}^{\mathrm{MW}}-\alpha\Delta\rho_{xx}^T|$. Further, we used only those data points with absolute values larger than the nonresonant signal $\alpha\Delta\rho_{xx}^T$. The resulting trace [solid line in Fig. 2(b)] is fitted by a Gaussian [dotted line in Fig. 2(b)]. The maxima of the Gaussians define the maxima positions used in the following.

In Fig. 3(a) the extracted resonance positions f_{res} are plotted vs B/B_0. Here, $B_0=2\hbar k_F/ea$ is the magnetic field for an orbit around one antidot, where k_F is the Fermi wave vector. $B_0=0.37$ T is experimentally obtained from ρ_{xx} measurements. The main resonance positions follow essentially the relation of a two-dimensional magnetoplasmon (2DMP): $f_{\mathrm{res}}=\sqrt{f_c^2+f_p^2}$ [dashed line in Fig. 3(a)], where $f_p(B=0)=59$ GHz is the plasmon frequency. Recent work[7] shows that collective effects are important even in 100-μm-wide Hall bars. Their dynamic response can be described by a localized 2DMP oscillation where the width of the Hall bar quantizes the wave vector of the plasmon $q=\pi/w$. From the graph f_{res}^2 vs B^2, with f_{res} taken from the antidot area, the plasmon frequency $f_p=59$ GHz is obtained from linear extrapolation to $B=0$. With the same method the effective mass of the 2DES, $m^*=0.071m_e$, is extracted from the slope. The horizontal bars in Fig. 3(a) mark the full width at half maximum (FWHM) obtained from the Gaussian line fit. The ρ_{xx} trace is shown in Fig. 3(b) for comparison. Here, arrows mark the positions of the expected classical commensurate orbits. The characteristic downbending of the lower branch ω^-, known from previous experiments on large antidot arrays,[1,8] is not observed here for frequencies up to 380 GHz. This deviation is characteristic for the transition from a classical cyclotron orbit around one antidot to an edge magnetoplasmon (EMP) mode. For an antidot diameter of 80 nm a magnetic field of $B\approx 1.9$ T would be necessary to come close to this transition, which requires frequen-

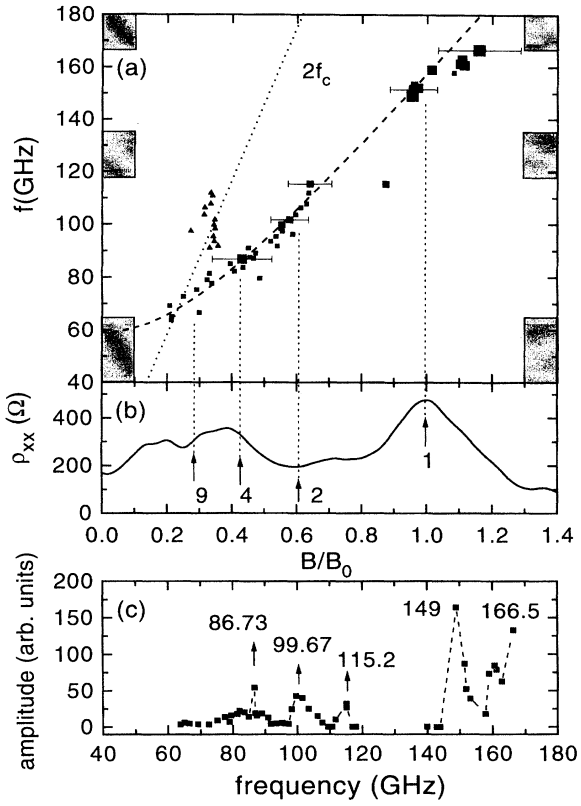

FIG. 3. (a) Dispersion f vs B/B_0 of the experimental resonance positions from the antidot system; the bars mark a few typical FWHM. The symbol size roughly illustrates the resonance amplitude. The gray fields on the left- and right-hand sides show the ranges where no microwave frequencies were available. Dashed line: calculated 2DMP dispersion for $f_p=59$ GHz with the effective electron mass $m^*=0.071m_e$. Dotted line: calculated cyclotron resonance line with $f=2f_c$. (b) ρ_{xx} taken at $T=1.3$ K; the arrows mark the classically calculated B positions of the commensurate orbits around 1, 2, 4, and 9 antidots, respectively. (c) Resonance amplitudes vs f obtained from normalization and Gaussian fit of the photosignals.

cies above 750 GHz. The most significant deviation of the resonances in Fig. 3(a) from the usual 2DMP dispersion is a lowering of the frequencies above $B/B_0\approx 1$. Although the FWHM becomes enlarged, the resonance maxima clearly shift to lower frequencies. The amplitude of the photosignal [Fig. 3(c)] has maxima near the magnetoresistance peaks of commensurate orbits around one and four antidots, while steadily rising towards an absolute maximum at $B/B_0=1$. We ascribe the first maximum at 86.7 GHz and $0.43B/B_0$ to the commensurate orbit around four antidots. Further, resonances that do not correspond to simple commensurate orbit peaks exist in the magnetic-field range between $0.5B/B_0$ and $0.7B/B_0$. At $0.63B/B_0$, the frequency tends to higher values than the 2DMP frequency. In the range of the magnetoresistance peaks corresponding to commensurate orbits around nine and four antidots [triangles at about $0.35B/B_0$ in Fig. 3(a)], we observe resonances with twice the cyclotron frequency $2f_c$. They can be observed over a large frequency range from 90 to 115 GHz. From other measurements, not shown here, we find for the commensurate orbits around four antidots and around one antidot at 130 GHz ($B/B_0\approx 0.4$) and at 350 GHz ($B/B_0\approx 1$), respectively, resonances with $2f_c$.

In order to confirm the interpretation of the experimental results we calculated the frequency-dependent conductivity in the antidot lattice. We model the antidot potential by[3]

$$U(x,y)=U_0\{\cos[(\pi/a)x]\cos[(\pi/a)y]\}^{\beta}, \tag{1}$$

where the even parameter β controls the steepness of the potential. The frequency-dependent conductivity, which is dominated by chaotic orbits, was calculated from the classical Kubo formula:[3]

$$\sigma_{ij}(\omega,\tau)=(1-p_p)\frac{ne^2}{k_BT}\int_0^{\infty} dt\; e^{(-1/\tau+i\omega)t}\langle \tilde{v}_i(t)\tilde{v}_j(0)\rangle_{\Gamma_c}, \tag{2}$$

where p_p is the phase-space fraction of pinned orbits and $\langle \tilde{v}_i(t)\tilde{v}_j(0)\rangle_{\Gamma_c}$ is the velocity correlation function of chaotic orbits averaged over phase space. The magnetoresistance ρ_{xx} calculated for $\beta=16$ by tensor inversion of Eq. (2) for

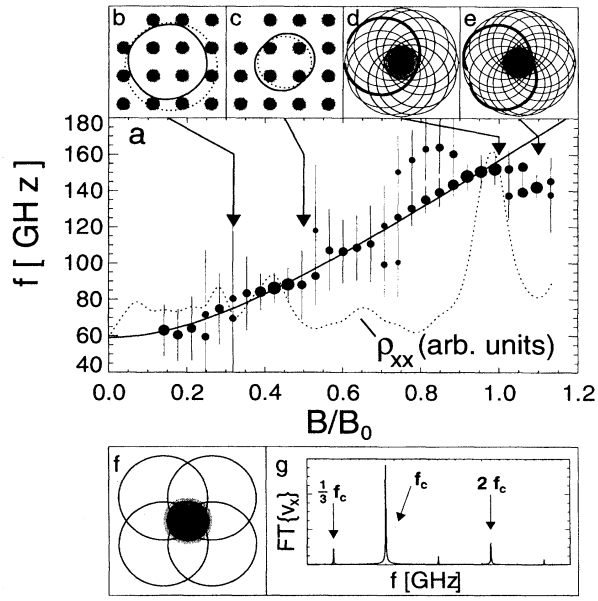

FIG. 4. (a) Calculated cyclotron resonance frequencies f_c for the model potential of Eq. (1) with $\beta=16$. The calculated magnetotransport curve $\rho_{xx}(B/B_0)$ (dotted line) for this β is in good agreement with the experimental curve of Fig. 3(b). The dots show the resonance frequency $f_{\rm res}$ vs B/B_0. Dot sizes indicate resonance height; vertical lines show the peak width at half maximum. The solid line is the MP dispersion of the unpatterned 2DES. (b) Periodic orbit at $B/B_0\approx 0.3$ (solid line) with reduced radius compared to the free cyclotron motion (dotted line), yielding an increased resonance frequency. (c) Periodic orbit at $B/B_0\approx 0.5$ (solid line) with increased radius compared to the free cyclotron motion (dotted line), yielding a reduced resonance frequency. (d) and (e) Periodic orbits at $B/B_0\approx 1.0$ and 1.1, respectively. The individual loops get more and more distorted by the antidot potential with increasing magnetic field, leading to reduced resonance frequencies. (f) Periodic orbit enclosing one antidot, with frequency ratio $\frac{1}{3}$, i.e., it encircles the antidot three times before it closes. (g) Frequency spectra of the orbit in (f). In addition to the main frequencies, i.e., the cyclotron frequency f_c and $\frac{1}{3}f_c$, harmonics show up due to the noncircular orbit.

$\omega=0$ is in good agreement with the experimental curve of Fig. 3(b). We thus compare the maxima of $\sigma(\omega,B)$ for this value of β with the experiment. A more detailed analysis of the theoretical findings, including calculations for different values of β, will be given in Ref. 10.

The resonance frequencies f_c are given by the relative maxima of the real part of $\{\sigma_{xx}\}$, calculated from Eq. (2). To compare with experiment we plot in Fig. 4(a) $f_{\rm res}=\sqrt{f_c^2+f_p^2}$ as a function of B/B_0, involving the experimentally obtained plasmon frequency f_p. The resonances are in good agreement with the experimental data. The calculated resonances stem from different classes of orbits including cyclotronlike motion around 1, 2, 4, and 9 antidots but also of more complicated periodic and quasiperiodic orbits. The resonances that lie far off the free cyclotron frequency in the magnetic-field range between $0.75B/B_0$ and $0.9B/B_0$ [Fig. 4(a)] are, for example, related to one complicated clover-shaped and unstable orbit. Such orbits require a perfect antidot potential and are thus unlikely to be observed in experiment. Here we focus on the magnetic-field ranges around $B/B_0\approx0.4$ and 1.0, where characteristic deviations from the cyclotron resonance of the free electron gas can be observed.

The peak in ρ_{xx} at $B/B_0\approx0.42$ is related to cyclotron orbits that encircle four antidots and the resonance lies exactly on the free cyclotron frequency. For slightly smaller magnetic fields these cyclotron orbits are deformed, as indicated in Fig. 4(b), with reduced radius, thus yielding slightly enhanced resonance frequencies. For magnetic fields slightly above $B/B_0\approx0.42$ the effective radius of the orbit is increased by the potential [see Fig. 4(c)], leading to a reduction of the resonance frequency. This crossover is also indicated in the experiment. The data points in Fig. 3(a) have a tendency to higher frequencies for magnetic fields left of $B/B_0\approx0.43$ and to lower frequencies on the right-hand side.

A similar crossover at $B/B_0\approx1.0$ evolves more clearly. Especially pronounced is the reduction of the resonance frequency between $B/B_0\approx1.0$ and 1.2, clearly observable both in the numerical calculations and in the experimental data. The understanding of this frequency reduction requires a precise description of the electron dynamics. So far, electron motion was only described in terms of periodic orbits. However, previous work shows that the main contribution to classical transport stems from chaotic orbits. Thus, while at, e.g., $B/B_0\approx1.1$ a circular cyclotron orbit located in the center of the nonlinear resonance still exists, the more complicated orbits become increasingly distorted by the antidots for $B/B_0>1$. Figures 4(d) and 4(e) show how the individual loops of these orbits get widened by the potential if the magnetic field is increased from $B/B_0=1.0$ to 1.1, thus yielding the reduction of the resonance frequency that is observed in the experiment.

Whereas the harmonic motion of the free cyclotron orbits is characterized by one single frequency, the frequency spectrum of a generic nonlinear oscillation shows harmonic frequencies, as is illustrated in Fig. 4(f) for a distorted cyclotronlike orbit in the antidot potential. In our model calculations we found significant resonances at twice the cyclotron frequency for $B/B_0\approx0.7$ to 1.2, in agreement with the experimental ones found at $B/B_0\approx1$ [not shown in Fig. 3(a)]. Within our model calculations no pronounced $2f_c$ resonances evolve at $B/B_0\approx0.35$ in contrast to the experiment [Fig. 3(a)]. This is not crucial to the comparison, however, since the actual strength of the $2f_c$ resonances depends strongly on the exact shape of the potential. Resonances and splittings of the MP dispersion at $2f_c$ have also been observed with FIR spectroscopy on 2DES,[11] in quantum dot[12] and antidot arrays,[1] and in quantum wires.[13–15]

In conclusion, we have presented the spectroscopic detection of commensurability effects in small antidot arrays, which we performed by a photoconductivity experiment. Model calculations based on the chaotic motion of electrons in an array of soft potential posts are in very good agreement with the experiments. The observed resonances with twice the cyclotron frequency are a direct consequence of the anharmonic motion of electrons in nonparabolic potentials.

We acknowledge useful discussions with R. Ketzmerick, K. Richter, V. Gudmundsson, B. Meurer, and G. Müller. We thank Y. Guldner and J. P. Vieren for supporting additional experiments at the Ecole Normale Supérieure, France. We also thank M. Riek, B. Schönherr, C. Lange, and F. Schartner for their expert help with the sample preparation. The sample was grown at Philips Research Laboratories, United Kingdom. This work was supported by the BMBF and the SFB Nichtlineare Dynamik.

[1] K. Kern, D. Heitmann, P. Grambow, Y. H. Zhang, and K. Ploog, Phys. Rev. Lett. **66**, 1618 (1991).

[2] D. Weiss, M. L. Roukes, A. Menschig, P. Grambow, K. von Klitzing, and G. Weimann, Phys. Rev. Lett. **66**, 2790 (1991).

[3] R. Fleischmann, T. Geisel, and R. Ketzmerick, Phys. Rev. Lett. **68**, 1367 (1992); Europhys. Lett. **25**, 219 (1994).

[4] H. Silberbauer and U. Rössler, Phys. Rev. B **50**, 11 911 (1994).

[5] J. F. Koch, Surf. Sci. **58**, 104 (1976).

[6] A. A. Bykov, G. M. Gusev, Z. D. Kvon, V. M. Kudryashev, and V. G. Plyukhin, Pis'ma Zh. Eksp. Teor. Fiz. **53**, 407 (1991) [JETP Lett. **53**, 427 (1991)].

[7] E. Vasiliadou, G. Müller, D. Heitmann, D. Weiss, K. von Klitzing, H. Nickel, W. Schlapp, and R. Lösch, Phys. Rev. B **48**, 17 145 (1993).

[8] B. Meurer, T. Deruelle, Y. Guldner, J. P. Vieren, M. Riek, K. von Klitzing, K. Eberl, and K. Ploog, Phys. Rev. B **49**, 16 813 (1994).

[9] Due to the zeros of $\Delta\rho_{xx}^T$, normalizing the photoconductivity signal by dividing by $\Delta\rho_{xx}^T$ would result in significant errors.

[10] R. Fleischmann *et al.* (unpublished).

[11] E. Batke, D. Heitmann, and J. P. Kotthaus, Phys. Rev. Lett. **54**, 2367 (1985).

[12] B. Meurer, D. Heitmann, and K. Ploog, Phys. Rev. Lett. **68**, 1371 (1992).

[13] T. Demel, D. Heitmann, P. Grambow, and K. Ploog, Phys. Rev. Lett. **66**, 2657 (1991).

[14] H. Drexler, W. Hansen, J. P. Kotthaus, M. Holland, and S. P. Beaumont, Phys. Rev. B **46**, 12 849 (1992).

[15] V. Gudmundsson, A. Brataas, P. Grambow, B. Meurer, Th. Kurth, and D. Heitmann, Phys. Rev. B **51**, 17 744 (1995).

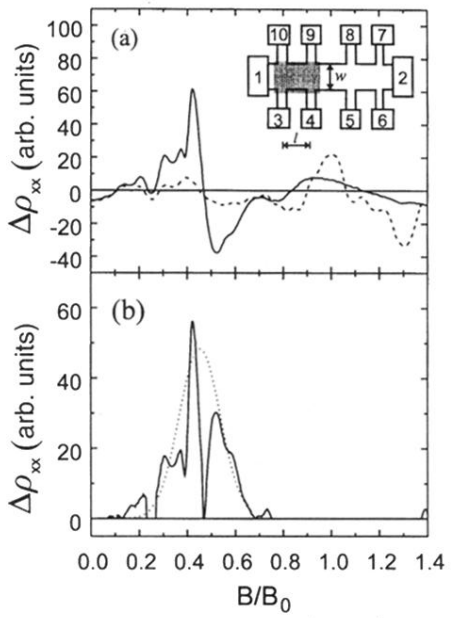

FIG. 2. Inset: Hall bar with patterned (shaded) and unpatterned segments. The period of the antidot lattice is $a=400$ nm and the geometrical antidot diameter is $d_{\mathrm{AD}}=80$ nm. Here, $w=100$ μm, $l=200$ μm, and $B_0=0.37$ T. (a) Dashed line: $\alpha\Delta\rho_{xx}^{T}=\alpha[\rho_{xx}(1.2\ \mathrm{K})-\rho_{xx}(4.2\ \mathrm{K})]$ matched to the photosignal $\Delta\rho_{xx}$ (solid line) for $f=86.7$ GHz. (b) Solid line: absolute value of the resonant part of the photosignal; dotted line: Gaussian fit used to determine the resonance position.

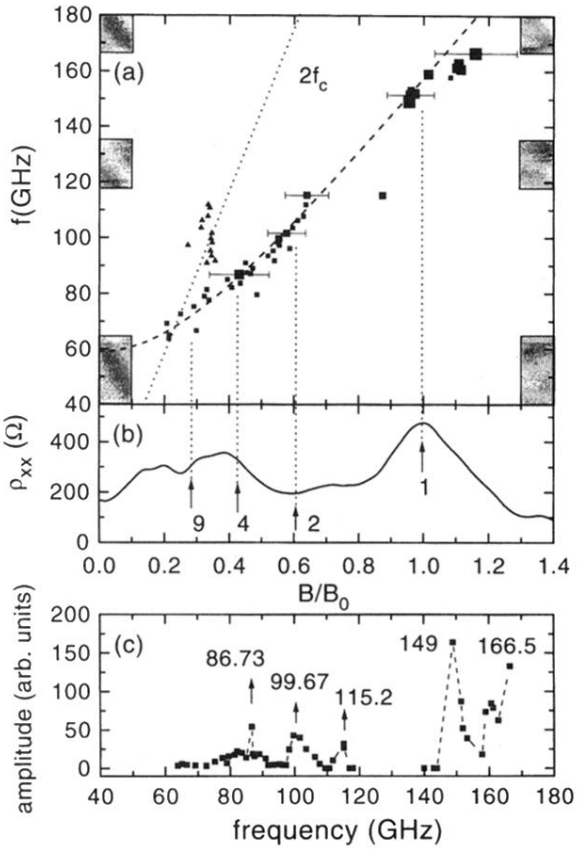

FIG. 3. (a) Dispersion f vs B/B_0 of the experimental resonance positions from the antidot system; the bars mark a few typical FWHM. The symbol size roughly illustrates the resonance amplitude. The gray fields on the left- and right-hand sides show the ranges where no microwave frequencies were available. Dashed line: calculated 2DMP dispersion for $f_p = 59$ GHz with the effective electron mass $m^* = 0.071 m_e$. Dotted line: calculated cyclotron resonance line with $f = 2f_c$. (b) ρ_{xx} taken at $T = 1.3$ K; the arrows mark the classically calculated B positions of the commensurate orbits around 1, 2, 4, and 9 antidots, respectively. (c) Resonance amplitudes vs f obtained from normalization and Gaussian fit of the photosignals.